RESEARCH REPORT

VTT-R-00023-24

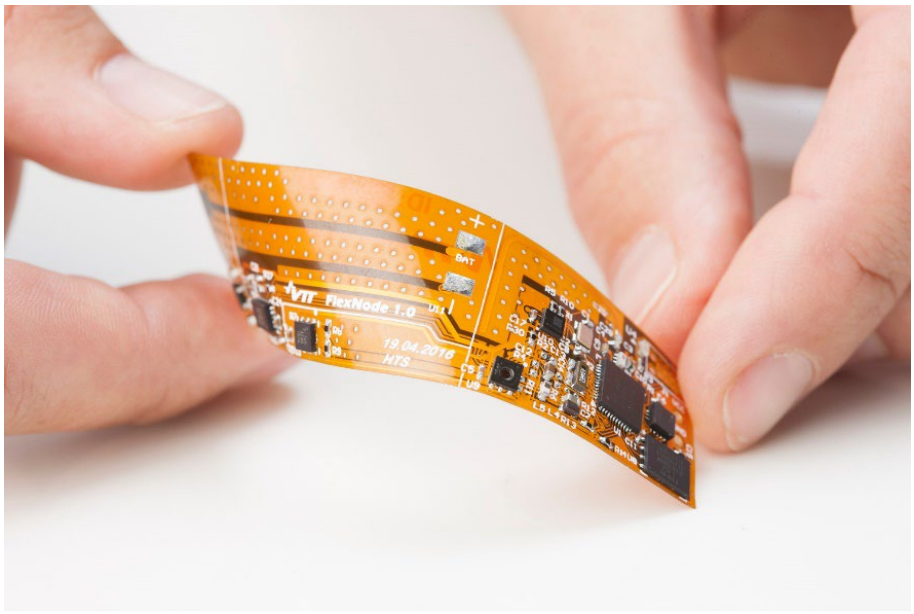

Assessment of alkali-silica reaction and aggressive aqueous attack in concrete 2023

Authors: Yushan GU

Confidentiality: VTT Public

Version: 7.2.2024

VTT

beyond the obvious

Report's title Assessment of alkali-silica reaction (ASR) and aggressive aqueous attack (AAA) in concrete 2023	
Customer, contact person, address National Nuclear Safety and Waste Management Research Programme SAFER2028	**Order reference** -
Project name Finnish Nuclear Concrete Ageing Management (FN-CAMP) Project, WP2	**Project number/Short name** 135900/FN-CAMP
Author(s) Yushan GU	**Pages** 19
Keywords Alkali-silica reaction; Aggressive aqueous attack; durability of concrete; modelling.	**Report identification code** VTT-R-00023-24

Summary

This report summarises the study that has been conducted in the SAFER2028 FN-CAMP project. The main objective of the WP2 of the project is to assess the deterioration mechanism induced by alkali-silica reaction (ASR) and aggressive aqueous attack (AAA) of concrete structures in nuclear power plants (NPPs). To achieve this goal, assessment tools to predict the ASR expansion of concrete and evaluate the deterioration of concrete exposed to an aggressive aqueous environment are developed within the project. The assessment tools are then validated by the existing literature data and explored in sensitivity analysis cases.

Confidentiality	VTT Public

Espoo 7.2.2024

Written by	**Reviewed by**
Yushan GU Research scientist	Pirkko Kekäläinen Research Scientist, FN-CAMP project manager

VTT's contact address
VTT Technical Research Centre of Finland Ltd., P.O. Box 1000, FI-02044 VTT, Finland

Distribution (customer and VTT)
SG3 of SAFER28
SG3 of the SAFER2028

Approval

VTT TECHNICAL RESEARCH CENTRE OF FINLAND LTD

Date:	8.2.2024
Signature:	Laitinen Tarja 912468625 Digitally signed by Laitinen Tarja 912468625 Date: 2024.02.09 08:08:00 +02'00'
Name:	Tarja Laitinen
Title:	Vice President, Knowledge-driven Design

Contents

1. Introduction

The SAFER2028 Finnish Nuclear Concrete Ageing Management (FN-CAMP) project aims to assess the safety performance of Finnish nuclear power plants (NPPs) and Finnish radioactive waste storage facilities (RWS), as their operations are required to be reviewed and updated constantly. Moreover, the project contributes to supporting the ageing related aspects based on the needs of Finnish End-Users, delivering outcomes in the form of assessment tools and providing guidelines for structural assessment and ageing management of civil engineering structures.

This report summarises the study that has been conducted in WP2 of the SAFER-FN-CAMP project during 2023. The main objective of the WP2 is to assess the deterioration mechanism induced by alkali-silica reaction (ASR) and aggressive aqueous attack (AAA) of concrete structures in NPPs. To achieve this goal, assessment tools for prediction of ASR expansion in concrete and evaluation of deterioration of concrete exposed to an aggressive aqueous environment are developed within the project. The assessment tools are then validated by the existing literature data and explored in sensitivity analysis cases.

2. WP2 Alkali-silica reaction (ASR) and aggressive aqueous attack (AAA) on structural performance

2.1 Task 2.1 ASR on structural performance

This task is to develop an assessment tool to evaluate the deterioration of concrete subjected to alkali-silica reaction (ASR). A thermo-chemo-cracking model (Saouma & Perotti, 2006) will be adopted to simulate the ASR expansion, with some parameters characterizing the material property. The main task for the year 2023 is to establish the assessment tool and replicate the expansion curves of concrete subject to ASR. The explanations of the tool are presented in section 2.1.2, and the validation of the model by the experimental data from the literature is reported in section 2.1.3.

2.1.1 Literature review

Alkali-aggregate reaction (AAR) was first identified as a cause of concrete deterioration by Stanton (Stanton, 1942). As a type of AAR, ASR is a chemical reaction among silica, alkali cations, and hydroxyl ions that are available in the pore solution of concrete. The reaction produces ASR gel that swells by absorbing moisture. The swelling results in internal stress that degrades the material. In the literature, modelling studies have been performed at multi-scales. (i) Micro-scale: the modelling at the micro-scale focuses on simulating the formation of ASR gel reacted from aggregates and cement pastes (Suwito, Jin, Xi, & Meyer, 2002) (Lemarchand, Dormieux, & Ulm, 2000). However, producing a proper database to simulate the amorphous gel is important and challenging. (ii) Meso-scale: size effect was the emphasis, which has been investigated in (Furusawa, Ohga, & Uomoto, 1994) (Bažant & Steffens, 2000). (iii) Macro-scale: numerical models analyze the structural performance from reaction kinetics (Léger, Côté, & Tinawi, 1996) (Huang & Pietruszczak, 1999), loading states (Charlwood, Solymar, & Curtis, 1992) (Thompson, Charlwood, Steele, & Curtis, 1994), impacts of temperature and moisture (Esposito & Hendriks, 2012) (Pesavento, Gawin, Wyrzykowski, Schrefler, & Simoni, 2012), etc. Models that couple chemical, thermal, and mechanical components have also been proposed, e.g., (Comi, Fedele, & Perego, 2009) (Capra & Sellier, 2003).

Among them, a model based on thermodynamics for expansion as a function of time was developed in (Larive, 1997), see Eq. (*1*). The equation describes a sigmoid curve expressing the volumetric expansion in time as a function of temperature and time. It includes parameters to be calibrated with the experimental

data and replicates the expansion curves, as illustrated in Figure 1. This model is a part of the thermo-chemo-cracking model we employ in the assessment tool.

$$\xi(t,\theta) = \frac{1 - e^{-\frac{t}{\tau_C(\theta)}}}{1 + e^{-\frac{t-\tau_L(\theta,I_\sigma,f_c')}{\tau_C(\theta)}}} \quad (1)$$

$$\tau_C(\theta) = \tau_C(\theta_0)\, exp[U_C(\frac{1}{\theta} - \frac{1}{\theta_0})] \quad (2)$$

$$\tau_L(\theta, I_\sigma, f_c') = f(I_\sigma, f_c')\, \tau_L(\theta_0) exp[U_L(\frac{1}{\theta} - \frac{1}{\theta_0})] \quad (3)$$

where τ_L is the latency time, corresponding to the inflexion point; and τ_C is the characteristic time defined as the intersection of the tangent at τ_L with the asymptotic unit value of ξ; U_L and U_C are the activation energies, i.e., the minimum energy required to trigger the reaction for the latency and characteristic times.

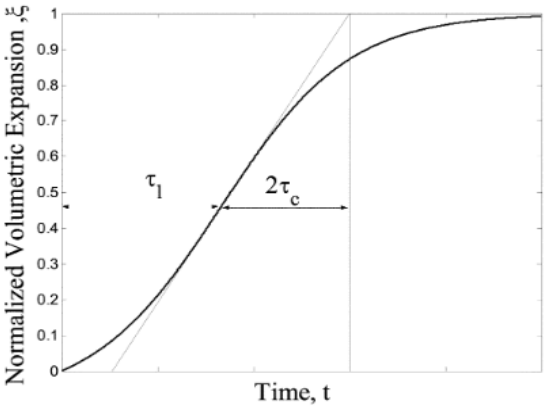

Figure 1: Normalised expansion curve ($\xi(t) = \varepsilon_{F,Vol}^{AAR}(t)/\varepsilon_{AAR}^{\infty}$).

2.1.2 Thermo-chemo-cracking model

An assessment tool based on the thermo-chemo-cracking model (Saouma & Perotti, 2006) was developed, and the code is implemented in the C programming language. The reason for choosing this model is that it couples the kinetics of the chemical reactions and the mechanics of cracking that affect volume expansion and the degradation of mechanical properties in a soft way. Moreover, the model can address the ASR anisotropy by assigning uniaxial, biaxial, and triaxial confining pressures and determining the distribution ratio of expansion in each case, and can accurately reproduce the expansion-strain evolution under multi-axial constraint conditions. It means that this comprehensive model considers the most important factors that influence ASR expansion, and it can be easily used by engineers and employed in industrial applications. Meanwhile, due to its simplification, the model is limited regarding the behaviour at the material scale. For example, the formation of ASR gel and the evolution of its microstructure cannot be addressed in this model, and crack generation is not included. To address these questions, models like (Sellier, Bourdarot, Multon, Cyr, & Grimal, 2009) (Takahashi, Tanaka, & Maekawa, 2018) (Morenon, et al., 2019) are recommended.

Our model simulates ASR as a volumetric expansion. Eq. (4) shows the incremental rate of the free volumetric strain in concrete subject to ASR, which considers the impacts of tensile cracking (Γ_t in Eq. (5)),

compressive stresses (Γ_c in Eq. (6)), relative humidity ($f(h)$ in Eq. (7)), normalised incremental expansion rate based on Eq. (1) ($\dot{\zeta}(t,\theta)$), and the laboratory-determined or predicted maximum free volumetric expansion at the reference temperature θ_0 ($\varepsilon^{\infty}|_{\theta=\theta_0}$). Eqs. (5) and (6) account for ASR reduction due to tensile cracking and compressive stresses, in which case gel is absorbed by generated microcracks. The chemical and mechanical components in the model are coupled via $\tau_L(\theta, I_\sigma, f_c')$, shown in Eq. (8), which takes the impact of temperature, expansion and mechanical states into account.

$$\dot{\varepsilon}_{vol}^{AAR}(t) = \Gamma_t(f_t', \sigma_1|COD) * \Gamma_c(\bar{\sigma}, f_c') * f(h) * \dot{\zeta}(t,\theta) * \varepsilon^{\infty}|_{\theta=\theta_0} \quad (4)$$

$$\Gamma_t = \begin{cases} 1 & if\ \sigma_l \le \gamma_t f_t' \\ \Gamma_r + (1-\Gamma_r)\dfrac{\gamma_t f_t^{fictitious}}{\sigma_I} & if\ \sigma_l > \gamma_t f_t' \end{cases} \quad (5)$$

$$\Gamma_c = \begin{cases} 1\ if\ \bar{\sigma} \le 0\ tension \\ 1 - \dfrac{e^{\beta}\bar{\sigma}}{1+(e^{\beta}-1)\bar{\sigma}} & if\ \bar{\sigma} > 0\ compression \end{cases} \quad (6)$$

$$f(h) = h^m \quad (7)$$

$$\tau_L(\theta, I_\sigma, f_c') = f(I_\sigma, f_c')\,\tau_L(\theta_0) exp[U_L(\frac{1}{\theta} - \frac{1}{\theta_0})] \quad (8)$$

$$f(I_\sigma, f_c') = \begin{cases} 1 & if\ I_\sigma > 0 \\ 1 + \alpha\dfrac{I_\sigma}{3f_c'} & if\ I_\sigma \le 0 \end{cases};\ I_\sigma = \sigma_I + \sigma_{II} + \sigma_{III} \quad (9)$$

$$\bar{\sigma} = \frac{\sigma_I + \sigma_{II} + \sigma_{III}}{3f_c'} \quad (10)$$

where Γ_r is a residual AAR retention factor for AAR under tension; γ_t is the fraction of the tensile strength beyond which gel is absorbed by the crack; σ_I is the maximum principal tensile stress; f_t is tensile strength; f_c' is the compressive strength; α is a parameter that was determined with a value of 4/3 in (Multon 2003).

Table 1 lists a summary of the parameters adopted in the model. Some values are referred to in the literature, while others are based on reasonable assumptions due to limited existing information in the literature. We assume the concrete structure under groundwater, i.e., relative humidity equals to 1. Thus, the parameters *h* and *m* have a value of 1.

Table 1: Summary of parameters used in the model.

U_L	9400 ± 500 K (Ulm, Coussy, Kefei, & Larive, 2000)	U_C	5400 ± 500 K (Ulm, Coussy, Kefei, & Larive, 2000)
θ_0	273 K	E_0	30 GPa
Γ_r	0.1	γ_t	0.9
f_t	3 MPa	f_c'	30 MPa
α	4/3 (Multon 2003)	β	0.5 (Saouma & Perotti, 2006)
h	1	*m*	1

2.1.3 Validation of the model

In this subsection, we implement the model to simulate the expansion curve reported in (Multon, 2003). As the first step, initial values of $\tau_C(\theta_0)$, $\tau_L(\theta_0)$, and ε^{∞} are given to the model. The model adjusts the values by comparing the predicted expansion to the experimental data and stops until their difference reaches a target criterion. We set a target criterion as 5e-4 in the calculation, so the implementation ends when the difference is less than 5e-4. Figure 2 presents a comparison of the simulated and measured data reported in (Multon, 2003). Table 2 summarizes the starting and final parameters, and the required iteration numbers when the target criterion regarding the difference is reached. From the table we can see, 61 iterations were needed to simulate the longitudinal expansion, and the characteristic and latency time were ended up with 78 and 128 days. In the case to simulate the transversal expansion, more iterations, i.e., 120 were implemented, and the final characteristic and latency time were ended up with 91 and 111 days.

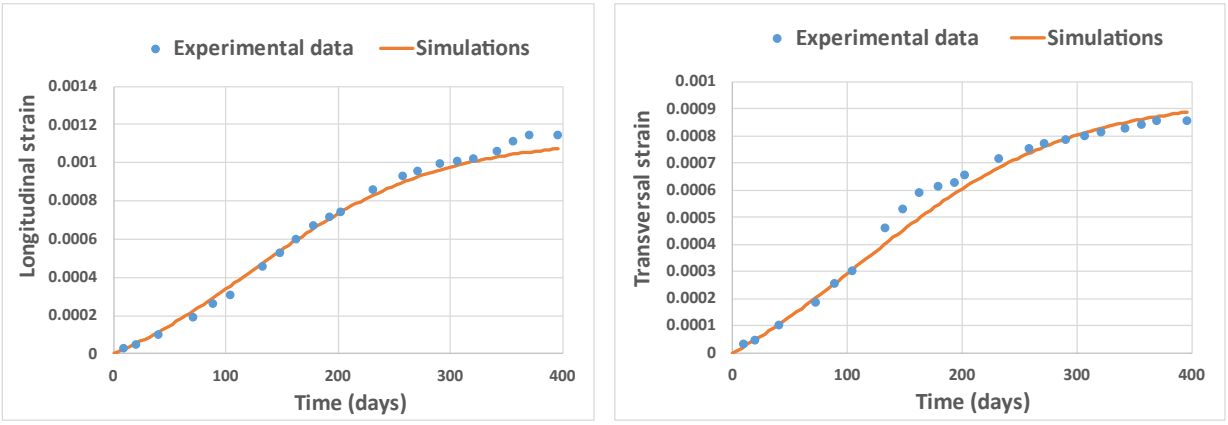

Figure 2: Simulated longitudinal (left) and transversal (right) expansion curve of concrete induced by ASR according to the experimental data reported in (Multon, 2003).

Table 2: Parameter identification and initial values.

	Time (days)		ε^{∞}	Iterations
	Characteristic $\tau_C(\theta_0)$	Latency $\tau_L(\theta_0)$		
Longitudinal expansion				
Initial	100	100	0.0010	-
Final	78	128	0.0011	61
Transversal expansion				
Initial	100	100	0.0010	-
Final	91	111	0.0009	120

It can be seen from Figure 2 that the proposed assessment tool well replicates the expansion curve of concrete subject to ASR. The latency and characteristic periods have been well represented by the proposed model. It is worth mentioning that we assumed the concrete under an isotropic state for the current study. To replicate the longitudinal and transversal strain mentioned above, we predicted two groups of volumetric strain independently and assumed the longitudinal/transversal strain in a portion of 1/3. However, the experimental data (Multon, 2003) tells us a different story, namely, the ASR expansion of concrete is anisotropic. The proposed tool can simulate the anisotropic case when we introduce a variable into the model, i.e., the weight of volumetric distribution. The variable distributes the volumetric expansion into three directions depending on the loading state. This part of the study has been planned within the FN-CAMP project, and the work will be done in the last project year when the impact of loading states is investigated.

2.2 Task 2.2 AAA on structural performance

An assessment tool based on reactive-transport modelling is developed in this task to evaluate the deterioration of concrete exposed to an aggressive environment, which includes pure water, sodium sulfate solution, groundwater, and seawater. This investigation order is determined according to the number of reactions that may occur between the material and the exposed solution. Leaching is the most fundamental phenomenon that will occur when concrete is exposed to a solution, and thus the performance of concrete exposed to pure water will be investigated as the first step. The investigative steps will be followed, in the order stated above, as described in the work plan within 3 years, and we believe it will help us better understand the deterioration mechanism of concrete. The obtained results contribute to making informed decisions on concrete performance, especially in the long term.

The main work regarding this sub-task in 2023 is to investigate the performance of concrete exposed to leaching. Leaching of calcium ions (Ulm, Torrenti, & Adenot, 1999) occurs when concrete is exposed to a solution. The corresponding consequences are (1) dissolution of portlandite (CH) and calcium silicate hydrate (C-S-H), which are the major components of concrete; (2) increase of the porosity due to the different molar volumes regarding reactants and products. This consequently accelerates the transport process that will accelerate the ion exchanges between material and surrounding solutions, and ultimately damage the material. In this sub-task, concrete exposed to pure water will be simulated, and the output include (1) the evolution of the mineral phases, pH, and porosity at a given location; and (2) the profile of

the mineral phases, pH, and porosity at a given time. The results will determine the degradation depth of concrete due to leaching, and the deterioration rate at different exposure durations, which will provide an assessment of the existing structures for extended service life.

2.2.1 Assessment tool

The reactive-transport modelling tool HP1, which couples Hydrus-1D with PHREEQC geochemical code, is used to predict the evolution and profile of mineralogical phases and pore water composition in the cementitious system. The material and geometry system are defined in Hydrus-1D, as well as boundary conditions. The boundary condition determines the way the exposed solution is transported. For example, when a constant concentration is imposed, Hydrus-1D transports the elements based on the gradient of concentration, namely, the diffusion process. However, when a constant flux/hydraulic gradient is imposed as a boundary condition, in addition to the diffusion process, a certain amount of solution in each cell is transported or replaced by the solution in the previous cell contrary to the flowing direction. For each transport step, chemical reactions are calculated based on the thermodynamic database maintaining the material system in an equilibrium state. The details of the simplified cement system, geometry, and input data are presented in this subsection.

2.2.1.1 Simplified cement model

The chemical processes involved are assumed to evolve under thermodynamic equilibrium. A thermodynamic database, CEMDATA v18 (Lothenbach, et al., 2019) (https://www.empa.ch/cemdata) – PHREEQC version is used to represent the cement system, where a comprehensive selection of cement hydrates on ordinary Portland cement and alkali-activated materials is available. Moreover, the equilibrium constants (i.e., log K values) for each equilibrium reaction under various conditions, standard molar volumes for each mineral, etc., are available in this thermodynamic database. The calcium silicate hydrate is considered ideal solid solutions with six end members (CSHQ-JenD, CSHQ-JenH, CSHQ-TobD, CSHQ-TobH, KSiOH, and NaSiOH), following the CSHQ model proposed in (Kulik, 2011). All cementitious materials are considered fully equilibrated as initial conditions in the reactive transport simulations. The cement hydration calculations have been carried out using the Gibbs energy minimization approach (with the GEM-Selektor software (Kulik et al., 2013)). It is worth noting that aggregates are considered chemically inert in the reactive transport model in this work, which means that aggregates are not involved in any chemical reactions.

The chemical reactions lead to porosity changes in cementitious materials due to the dissolution/ precipitation of phases, which changes the permeability property of the cementitious barrier. Therefore, the porosity and permeability feedback are considered important factors when simulating the chemical evolution in a massive concrete structure. When considering the feedback, the porosity is updated in each time step of the chemical calculations by adding the precipitated phases and removing the dissolved ones in volume fraction. The resulting change of porosity is then transferred to the transport equations as feedback and the corresponding diffusive properties are updated.

2.2.1.2 Simplified geometry

The reactive transport model considers the cementitious system in an initially fully saturated state, and the material has been conceptualized as homogeneous porous media. The schematic layout of the system is presented in Figure 3. The total length of the considered cementitious system is 1 m, and it is divided into 10 elements with Δx=0.1 m. Boundary conditions (BD) are imposed on two sides of the system, which can be defined as a constant concentration, a constant flux, and even variable cases depending on the simulating scenarios. The initial composition of the exposed solution, initial phases, and composition of pore solution in mortar are required to be defined as input, which will be explained in section 2.2.2.1.

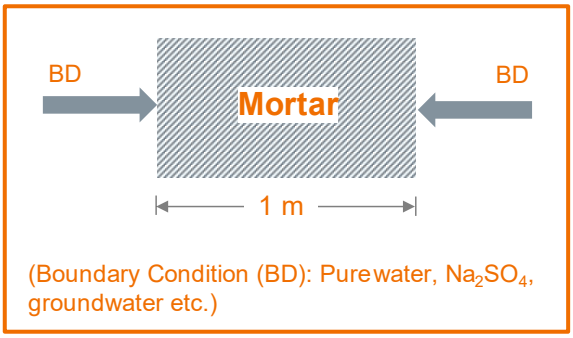

Figure 3: Schematic layout of the simulated cementitious system and the surrounding boundary conditions.

2.2.1.3 Input data

Cementitious materials are considered fully equilibrated as initial conditions in the reactive transport simulations. The fully hydrated mortar/concrete includes portlandite, CSHQ, and calcite ($CaCO_3$) as the main minerals, and the C-S-H solid solution shows a relatively higher amount of the JenD (Ca/Si=2.25) and TobD (Ca/Si=1.25) end members. The equilibrated pore water in mortar shows a highly alkaline pH due to the high concentrations of Na and K. The calculated porosity of the mortar is 29% based on the cement hydration calculations. A pore diffusion coefficient of 1.0E-9 m^2/s is selected, which considers the high interconnection of the pore structure in the mortar and a corresponding high impact on transport property. Table 3 summarizes the initial mineral phases present in the cementitious materials, and Table 4 shows the composition of the pore solution in mortar. The input data is referred to in an investigation case in the EURAD-ACED project (Samper, et al., 2022).

Table 3: Initial mineral phases in cementitious materials (Samper, et al., 2022).

Mineral [mol/kg water]	Mortar
CSHQ-JenD	1.5092
CSHQ-JenH	0.9835
CSHQ-TobD	1.1345
CSHQ-TobH	0.0486
KSiOH	0.1340
NaSiOH	0.0420
Ettringite	0.1207
Monocarbonate	0.2092
Calcite	0.2445
$C_3FS_{0.84}H_{4.32}$	0.1460
Portlandite	3.6971
Hydrotalcite	0.0822

Table 4: Composition of the pore solution in cementitious materials (Samper, et al., 2022).

Species [mol/L]	Mortar
pH	13.09
pe	-6.8
Ca	2.65e-3
Mg	2.94e-9
Na	9.13e-3
K	1.53e-1
Fe	4.98e-8
Al	3.30e-5
Cl^-	1.95e-7
C(4)	3.33e-5
S(6)	5.54e-4
Si	3.79e-5
Sr	1.00e-10

The interaction with surrounding environment is simplified to a constant diffusion / diffusion-advection of exposure solution on the boundaries with/without a hydraulic gradient. When hydraulic gradient is not considered, diffusion will be the only process influencing the chemical evolution in the system. In the case of considering a hydraulic gradient, a coupled process of advection and diffusion will occur. A hydraulic gradient of 0.026773 is applied with a pressure head of 0.026773 m on the left and 0 on the right within a distance of 1 m. The calculations are based on assumptions of a slow groundwater flow rate of 2.33E-13 m/s and a hydraulic conductivity of 8.72E-12 m/s in the granite (Samper, et al., 2022)(Samper, et al., 2021).

2.2.2 Simulated mineralogical profiles of the cementitious system

2.2.2.1 Simulations of the system in initial state

Figure 4 shows the initial state of the mineralogical phases in the system, where the aggregate in mortar is represented by the inert phase (marked in grey) and the empty space represents the porosity. The pH value is shown on the secondary axis on the right, which has a highly alkaline pH above 13 at the initial state. The mineralogical evolutions in two cases will be investigated in this section: (i) a case without considering hydraulic gradient, where diffusion is the only process; and (ii) another case with considering hydraulic gradient, where both diffusion and advection will occur.

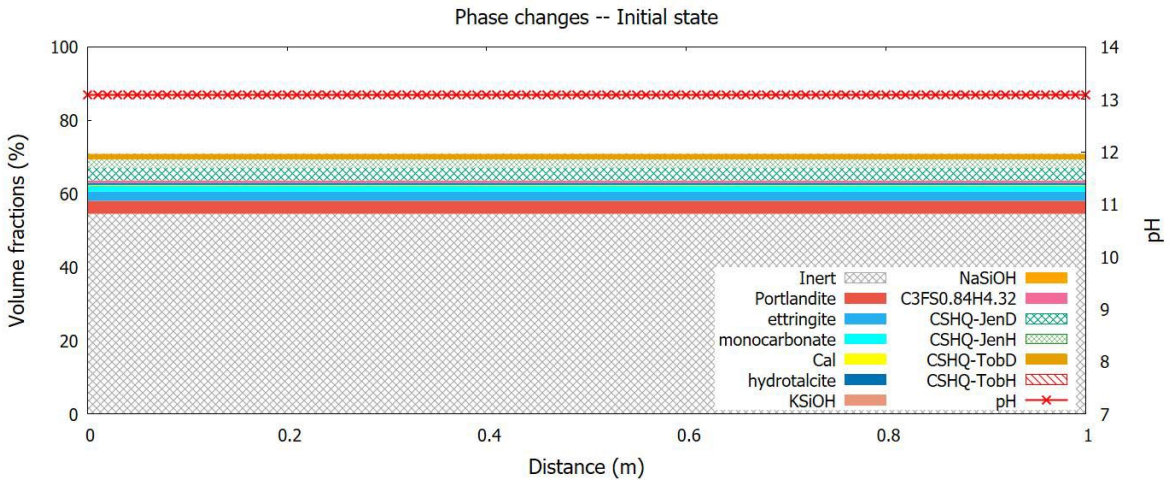

Figure 4: Initial mineralogical phases present in the considered cementitious system.

2.2.2.2 Simulations without considering hydraulic gradients (Diffusion)

Due to the concentration gradient of elements in pore solutions at the interface, chemical reactions are initiated leading to chemical gradients, as shown in Figure 5. The figures show the evolution of mineralogical phases and the pH in the system after being exposed for up to 5,000 years, after which the calculation was stopped as all cementitious material was consumed up. The main degradation phenomenon occurring in cementitious material is the dissolution of portlandite, the decalcification of C-S-H, followed by the dissolution of other phases. These reactions lead to an increase in porosity due to the difference in molar volume regarding reactants and products.

The pH value of the cementitious material drops from an initial value above 13 along the degradation. The decrease of pH values is due to the interaction with exposure solution, e.g., leaching of species from cementitious material to the surrounding environment. The pH values in the region close to the border of the considered system reach 7 due to a low pH value defined in the exposure solution. Then the pH values in middle parts decrease continually. This can be confirmed by the evolution of the composition in mortar pore solution presented in Figure 6. The concentration of Ca in the pore solution of mortar decreases due to the dissolution of CH and decalcification of C-S-H, and the leaching from cementitious material to the exposure solution. However, the concentration of Cl, K, and Na dropped rapidly approaching 0.

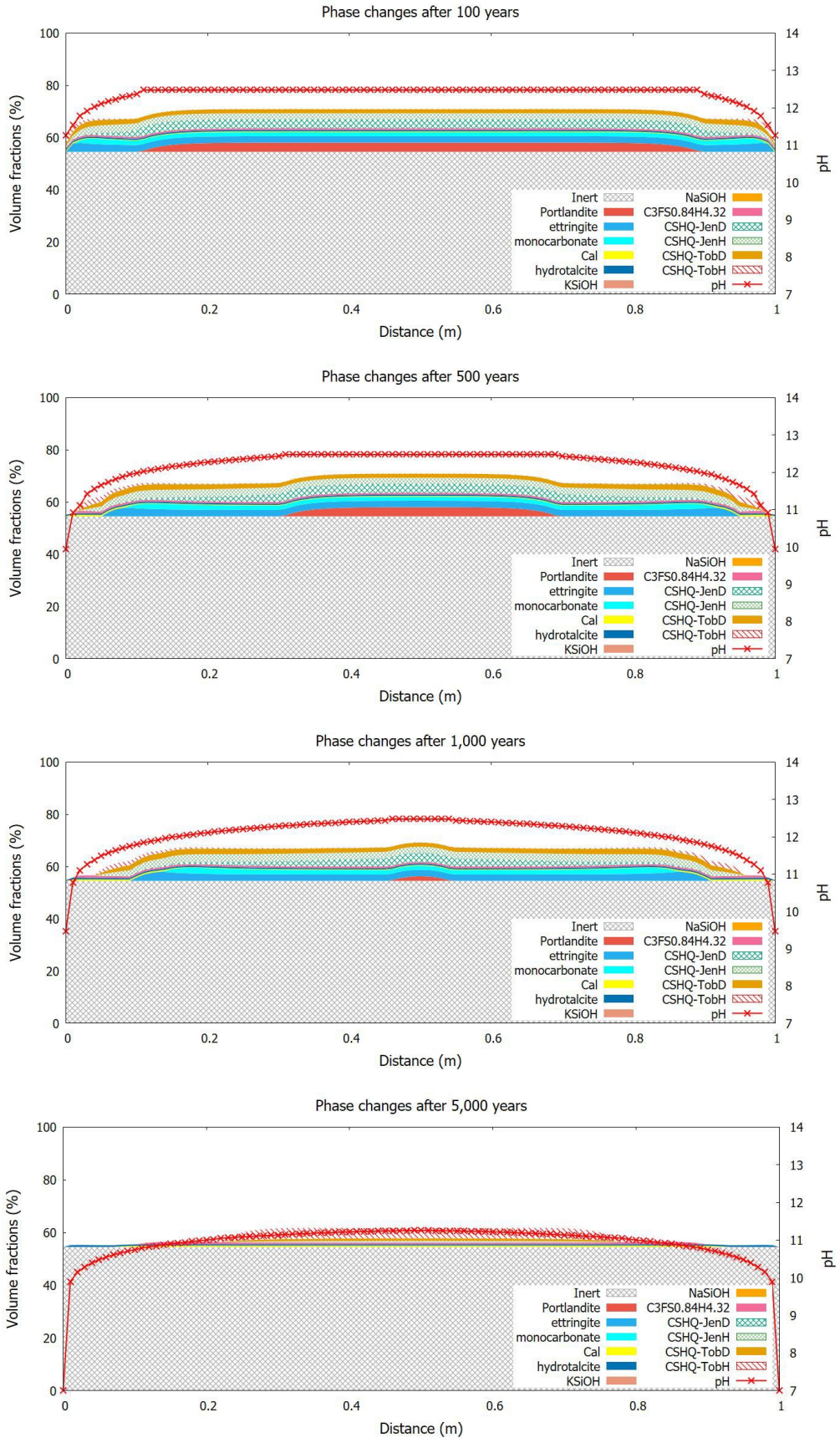

Figure 5: Mineralogical profiles of the cementitious system exposed to pure water (no hydraulic gradient) for up to 5,000 years.

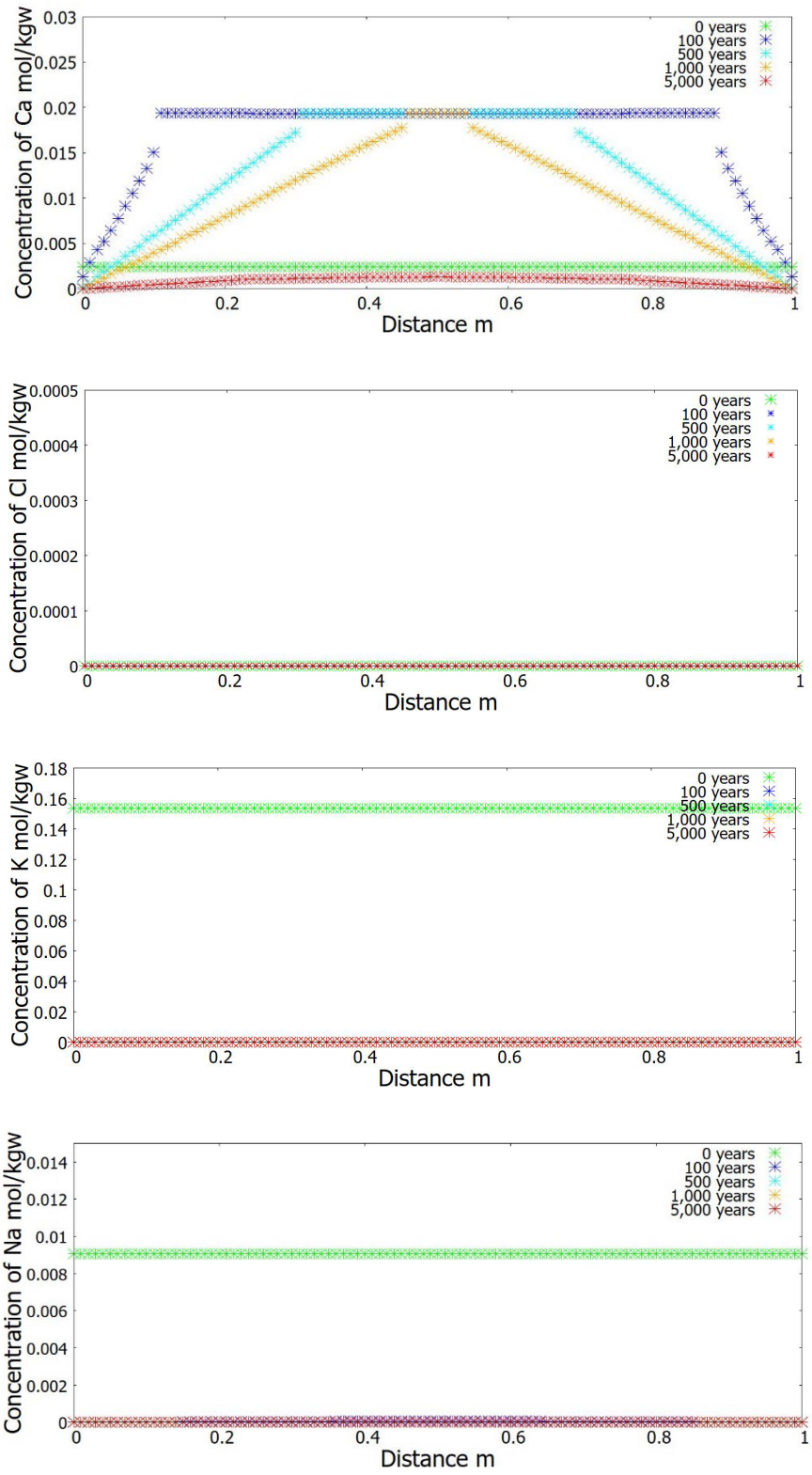

Figure 6: Concentration profiles regarding (a) Ca, (b) Cl, (c) K, and (d) Na in the cementitious system exposed to pure water without considering hydraulic gradients.

2.2.2.3 Simulations with considering hydraulic gradients (Diffusion + Advection)

Figure 7 presents the mineralogical evolution of the system when a hydraulic gradient is applied. In addition to diffusion, the advection process is foreseen influencing the chemical evolution. Due to the ingress of

exposure solution and the concentration gradient of elements in pore solutions at the interface, chemical gradients are created. First of all, the degradation phenomenon is similar compared to the case where the hydraulic gradient is not considered, namely, the dissolution of phases and the precipitation of calcite. However, the degradation rate of concrete is significantly faster. The cementitious material is observed fully dissolved before being exposed for 1,000 years, a similar degradation degree was found in the previous case when the cementitious material was exposed for up to 5,000 years. The pH value is observed to drop to 7 starting from the border area of the system. Secondly, the mineralogical profiles are not symmetrical, which means that the advection process is playing a dominant role compared to the diffusion process. The impact of solution flow depends on the hydraulic gradient considered in the model, i.e., a higher hydraulic gradient leads to a faster flow of solution and thus a more dominant advection process. This is an extremely important factor when considering a massive concrete structure exposed to a geological scenario, e.g, choosing a site for NPPs and repositories. A non-symmetrical profile regarding the concentration of Ca is observed in Figure 8, while the concentration of Cl, K, and Na decreases rapidly in the system due to leaching, which is similar to the case discussed previously.

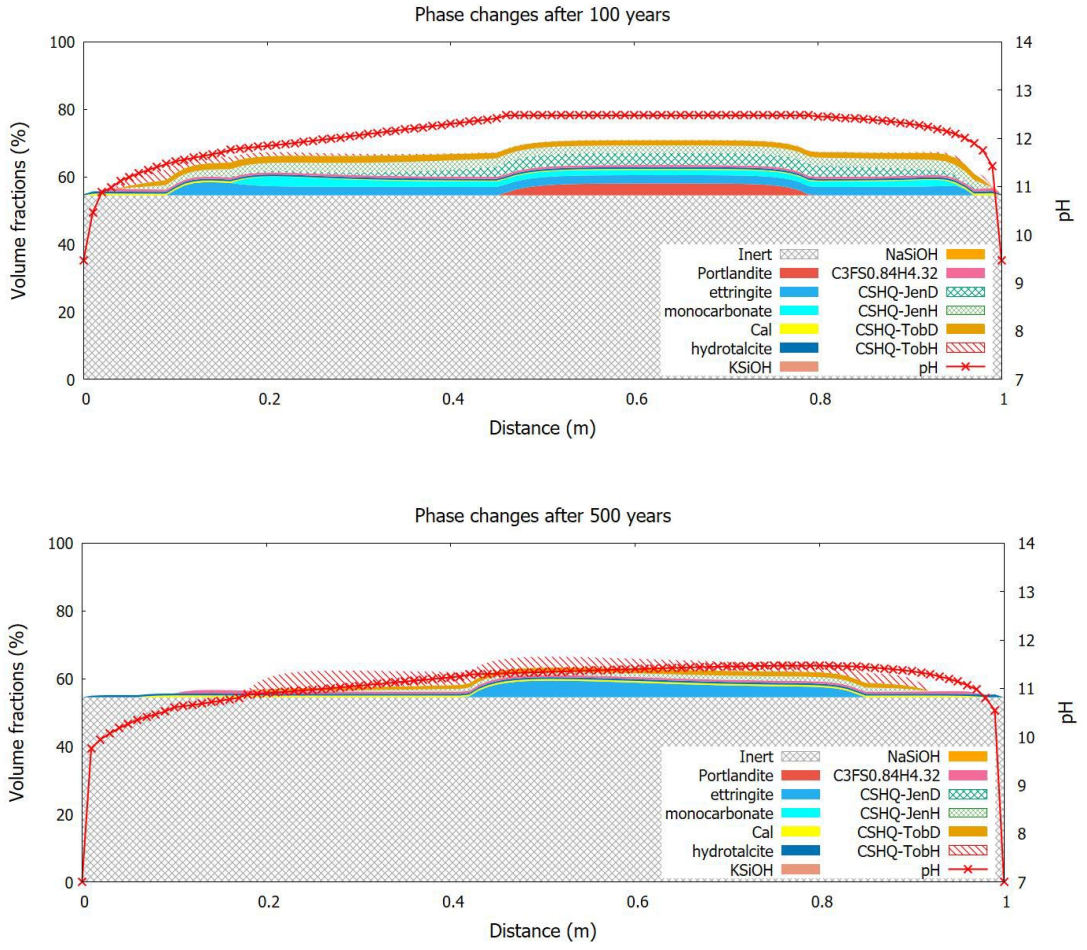

Figure 7: Mineralogical profiles of the cementitious system exposed to pure water (with hydraulic gradient) for up to 500 years.

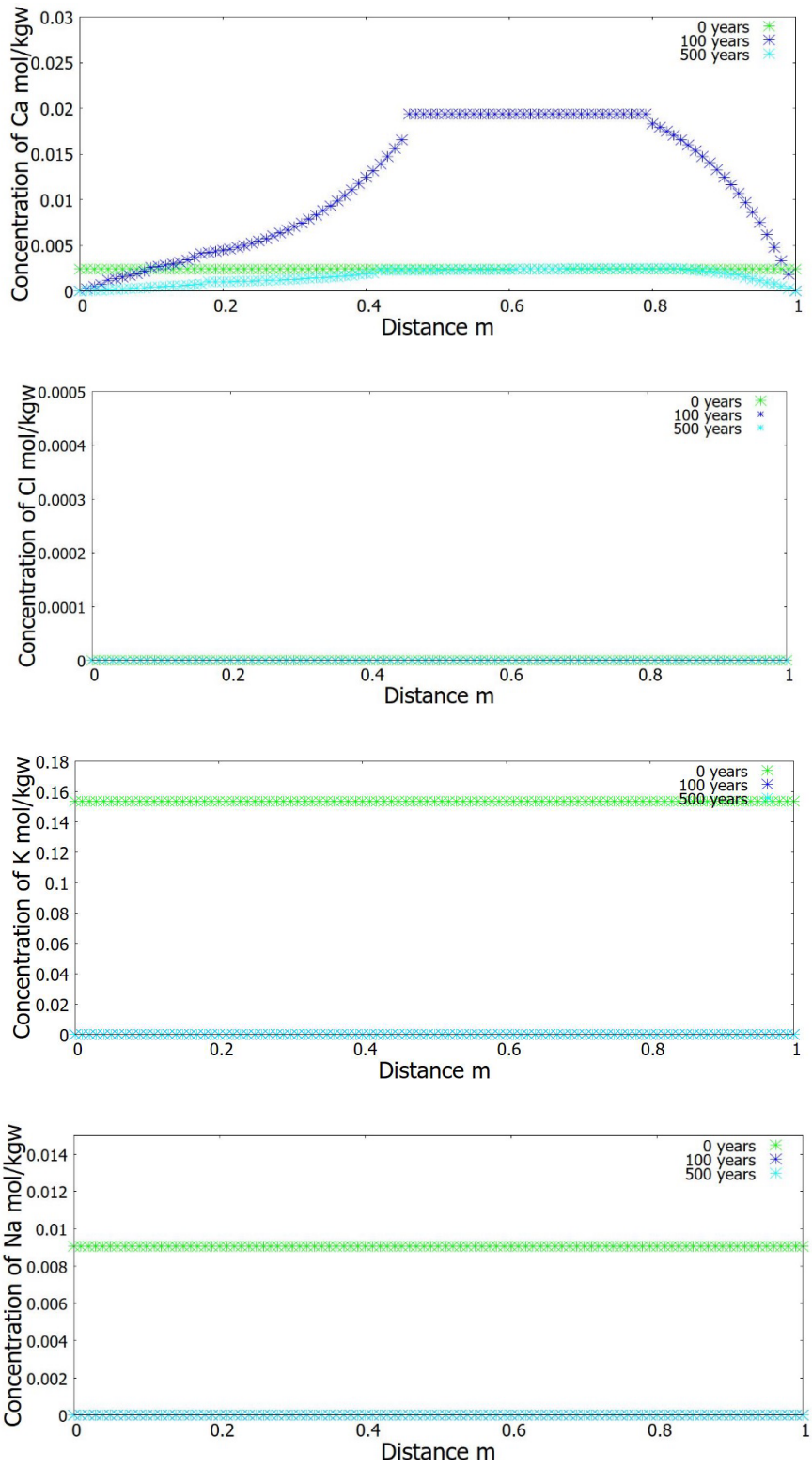

Figure 8: Concentration profiles regarding (a) Ca, (b) Cl, (c) K, and (d) Na in the cementitious system.

3. Conclusions and summary

This report summarised the work that has been done in the WP2 of the SAFER-FN-CAMP project during 2023. An assessment tool based on the thermo-chemo-cracking model to predict the performance of concrete subject to alkali-silica reaction has been developed in the first task. The model considers the impact of tensile cracking, compressive stresses, relative humidity, normalized incremental expansion rate, and the laboratory-determined maximum free volumetric expansion. By providing the initial characteristic time $\tau_C(\theta_0)$ and latency time $\tau_L(\theta_0)$ as input, the model predicts the expansion as a function of time. The model adjusts the values of $\tau_C(\theta_0)$ and $\tau_L(\theta_0)$ by comparing the predicted expansion to the experimental data, and stops the iteration until the difference reaches a target criterion. The tool has been preliminarily validated by the literature data. However, the anisotropic state of the ASR expansion cannot be correctly predicted by the model for the moment. The longitudinal and transversal strain were calculated as 1/3 of the volumetric expansion. In the following steps, sensitivity analyses on the model will be performed to better understand the developed assessment tool. Moreover, the impact of loading states on expansion will be analyzed in the project at the end.

In the second task, an assessment tool based on the reactive-transport modelling to predict the deterioration of cementitious material exposed to pure water or leaching has been proposed. It was observed that cementitious phases dissolve starting from portlandite followed by C-S-H and other phases, with calcite precipitating. The degradation of the mortar increases porosity due to the volume changes regarding reactants and products, which accelerates the transport and consequently the deterioration. Two cases were investigated: (i) a constant concentration as the boundary condition, where the hydraulic gradient was not considered and only the diffusion process was simulated; and (ii) a constant concentration and ingress of solution as the boundary condition, where the hydraulic gradient and a coupled diffusion-advection process was simulated. The deterioration rate of mortar in the second case was observed much faster compared to the first case, which indicates an important impact of the advection. It was further confirmed by the asymmetric profiles regarding mineralogical phases in the cementitious system. However, the impact degree depends on the hydraulic gradient we considered in the model. In the next steps, the performance of cementitious material exposed to a more complicated scenarios will be simulated and investigated, i.e., sulfate solution and groundwater, which will provide us a better understanding of concrete when it is exposed to a more aggressive aqueous environment.

References

Bažant, Z., & Steffens, A. (2000). Mathematical model for kinetics of alkali–silica reaction in concrete. *Cement and concrete research, 30*(3), 419-428.

Capra, B., & Sellier, A. (2003). Orthotropic modelling of alkali-aggregate reaction in concrete structures: numerical simulations. *Mechanics of materials, 35(8)*, 817-830.

Charlwood, R., Solymar, S., & Curtis, D. (1992). A review of alkali aggregate reactions in hydroelectric plants and dams. *In Proceedings of the international conference of alkali-aggregate reactions in hydroelectric plants and dams.*

Comi, C., Fedele, R., & Perego, U. (2009). A chemo-thermo-damage model for the analysis of concrete dams affected by alkali-silica reaction. Mechanics of materials. *41(3)*, 210-230.

Esposito, R., & Hendriks, M. (2012). A Review of ASR modeling approaches for Finite Element Analyses of dam and bridges. *In 14th International Conference on Alkali Aggregate Reaction.*

Furusawa, Y., Ohga, H., & Uomoto, T. (1994). Analytical study concerning prediction of concrete expansion due to alkali-silica reaction. Special Publication. *145*, 757-780.

Huang, M., & Pietruszczak, S. (1999). Alkali-silica reaction: modeling of thermo-mechanical effects. Journal of Engineering Mechanics. 476-487.

Kulik, D. (2011). Improving the structural consistency of C-S-H solid solution thermodynamic models. *Cement and Concrete Research, 41*, 477–495.

Larive, C. (1997). Apports combinés de l'expérimentation et de la modélisation à la compréhension de l'alcali-réaction et de ses effets mécaniques. *Doctoral dissertation, Ecole nationale des ponts et chaussees*.

Léger, P., Côté, P., & Tinawi, R. (1996). Finite element analysis of concrete swelling due to alkali-aggregate reactions in dams. *Computers & structures, 60*(4), 601-611.

Lemarchand, E., Dormieux, L., & Ulm, F. (2000). A micromechanical approach to the modeling of swelling due to alkali-silica reaction. *14th Engrg. Mech. Conf.*

Lothenbach, B., Kulik, D., Matschei, T., Balonis, M., Baquerizo, L., Dilnesa, B., Myers, R. (2019). Cemdata18: a chemical thermodynamic database for hydrated Portland cements and alkali-activated materials. *Cement Concrete Research, 115*, 472–506.

Morenon, P., Multon, S., Sellier, A., Grimal, E., Hamon, F., & Kolmayer, P. (2019). Flexural performance of reinforced concrete beams damaged by Alkali-Silica Reaction. *Cement and Concrete Composites, 104*, 103412.

Multon, S. (2003). Evaluation expérimentale et théorique des effets mécaniques de l'alcali-réaction sur des structures modèles. *Doctoral dissertation, Marne-la-Vallée*.

Pesavento, F., Gawin, D., Wyrzykowski, M., Schrefler, B., & Simoni, L. (2012). Modeling alkali–silica reaction in non-isothermal, partially saturated cement based materials. *Computer Methods in Applied Mechanics and Engineering, 225*, 95-115.

Samper, J., Montenegro, L., De Windt, L., Montoya, V., Garibay-Rodríguez, J., Grigaliuniene, D., Cochepin, B. (2022). Conceptual model formulation for a mechanistic based model implementing the initial SOTA knowledge (models and parame) in existing numerical tools.

Samper, J., Montenegro, L., De Windt, L., Montoya, V., Garibay-Rodríguez, J., Grigaliuniene, D., Poskas, P. (2021). Conceptual model formulation for a mechanistic based model implementing the initial SOTA knowledge (models and parameters).

Saouma, V., & Perotti, L. (2006). Constitutive model for alkali-aggregate reactions. *ACI materials journal*, 103(3):194.

Sellier, A., Bourdarot, E., Multon, S., Cyr, M., & Grimal, E. (2009). Combination of structural monitoring and laboratory tests for assessment of alkali-aggregate reaction swelling: application to gate structure dam. *ACI materials journal, 106*(3), 281-290.

Stanton, T. (1942). Expansion of concrete through reaction between cement and aggregate. *Transactions of the American Society of Civil Engineers*, 107(1):54-84.

Suwito, A., Jin, W., Xi, Y., & Meyer, C. (2002). A mathematical model for the pessimum size effect of ASR in concrete. *Concrete Science and Engineering, 4*(13), 23-34.

Takahashi, Y., Tanaka, Y., & Maekawa, K. (2018). Computational life assessment of ASR-damaged RC decks by site-inspection data assimilation. *Journal of Advanced Concrete Technology, 16*(1), 46-60.

Thompson, G., Charlwood, R., Steele, R., & Curtis, D. (1994). Mactaquac generating station intake and spillway remedial measures,. *In Proceedings of the 18th International Congress on Large Dams, 1*, 347-368.

Ulm, F., Coussy, O., Kefei, L., & Larive, C. (2000). Thermo-chemo-mechanics of ASR expansion in concrete structures. Journal of engineering mechanics. *126*(3), 233-242.

Ulm, F.-J., Torrenti, J.-M., & Adenot, F. (1999). Chemoporoplasticity of calcium leaching in concrete. *Journal of Engi-neering Mechanics, 125*(10), 1200–1211.